*Journal of Structural Geology*, Vol. 13, No. 1, pp. 71 to 86, 1991
Printed in Great Britain

0191-8141/91 $03.00+0.00


# Folding and shear deformation in quartzites, inferred from crystallographic preferred orientation and shape fabrics

HOLGER STÜNITZ*

Geologisches Institut, ETH-Zentrum, 8092 Zürich, Switzerland

(*Received* 14 *November* 1989; *accepted in revised form* 3 *April* 1990)

**Abstract**—Folding and simple shear deformation frequently occur together on all scales. The kinematic information from crystallographic preferred orientation (CPO) and microstructural information from shape fabrics are used to investigate the relationships of simple shear and folding in small-scale folds.

Three fold samples were analysed: sample 1 with the fold axis perpendicular; sample 2 oblique; and sample 3 essentially parallel to the shear direction. All folds have formed by buckling in a simple shear deformation regime. The principal kinematic directions for each sample lie in a single plane normal to the fold axial plane and at variable angles to the fold axis. The CPOs allow a distinction to be identified between coaxial and simple shear deformation components in different parts of each fold. The shear senses determined by CPOs and shape fabrics indicate that the shear deformation and the buckling of the layers occurred approximately simultaneously in all samples. CPO analysis of the flexural-slip components of the folding suggests that the fold axes have not rotated substantially towards the extension direction since their initiation. The variable orientations of the fold axes are explained by variable original orientations of the anisotropy with respect to the shear direction.

## INTRODUCTION

REGIONS of strong shear deformation frequently exhibit intensive folding. The term 'shear deformation' is chosen here as a more general term than 'simple shear' to describe a deformation that consists predominantly of simple shear components, but which may also include components of coaxial deformation. Usually, the folds in such regions display a reorientation of fold axes towards the finite extension direction, or they may even be sheath folds (Sanderson 1973, Escher & Watterson 1974, Cobbold & Quinquis 1980). In the study presented here, however, the folds were sampled in a region where many fold axes are subparallel or mildly oblique to the shear direction, but strongly curved fold axes and sheath folds are absent. Thus, an extensive rotation of initial folds, during subsequent shear deformation, is unlikely.

In order to analyse the relationships between folding and simple shear deformation components, the microstructures of three samples of folded quartzite layers have been analysed for their crystallographic preferred orientation (CPO) and shape fabrics.

Quartz *c*-axes in folds have been measured in a number of studies (Sander 1931, p. 257, Ladurner 1951, Jones 1959, Ball 1960, Dhonau 1961, Gangopadhyay & Johnson 1962, Carreras *et al.* 1977, Price 1981). However, except for the studies of Carreras *et al.* (1977) and Price (1981), these investigations were made before the kinematic significance of quartz *c*-axis pole figures was known. The main purpose of the earlier studies was to demonstrate that the folds could be 'unfolded'. The results of the CPO and the surface ODF in this present study are different from those of the previous ones and are used to establish the time sequence and kinematic relationships of shear deformation and folding.

## SAMPLE DESCRIPTION

The samples were taken in the vicinity of M. Nery in the Central Sesia Zone, Western Alps. The region underwent a polyphase folding history in which four phases of folding can be distinguished (Passchier *et al.* 1981, Stünitz 1989). The analysed folds are $F_2$ structures unmodified by the later folding events. Deformation occurred under greenschist-facies *P–T* conditions. Sample 1 was taken from a gneiss, samples 2 and 3 from a schist.

The location of sample 1 is about 1 km away from samples 2 and 3. These samples were selected because the fold axes of samples 1, 2, and 3 are normal, oblique and subparallel to the lineations and kinematic directions, respectively, and the samples exhibit different lithologies. The comparison of the three samples is justified by their relative proximity and by the fact that the shear deformation occurred in the same regional kinematic framework during the same event ($F_2$). The regional implications of this study are the subject of a separate paper and, therefore, all details of a regional framework have been omitted. The kinematic reference framework deduced from the samples applies only to the fold geometry and lineation orientation of each individual sample.

Sample 1 is an almost pure quartzite layer (0.5–1 cm thick) within a predominantly albite + zoisite matrix which contains some quartz and chlorite (Fig. 1a). A lineation is orientated parallel to the fold axis. The nature of the lineations will be discussed below. Samples

*Present address: Geologisch-Paläontologisches Institut, Universität Basel, Bernoullistrasse 30–32, 4056, Basel, Switzerland.

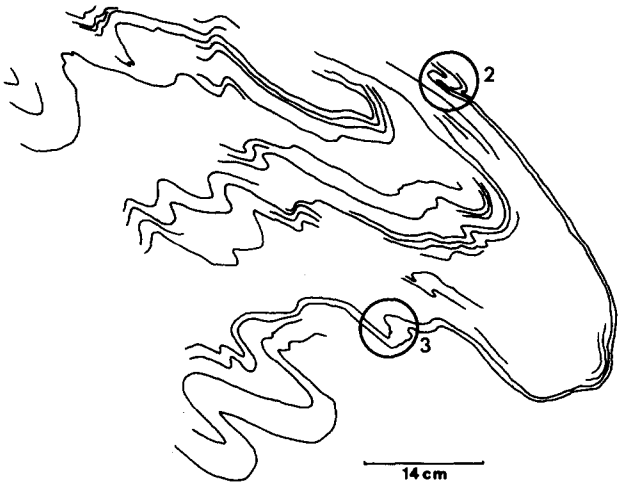


Fig. 2. Locations of the two fold samples 2 and 3 in the higher order fold. Both samples are viewed approximately down the fold axis, but show fold axis variations of about 20° with respect to the higher order fold. They represent S- and Z-shaped parasitic folds on either limb of the larger scale fold.

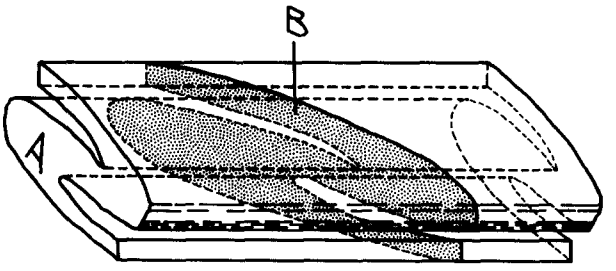


Fig. 3. Schematic drawing of sample 2, showing the plane A perpendicular to the fold axis and plane B (shaded), which is defined by the different directions of the lineation across the fold. The plane B is the plane in which CPO diagrams and shape fabric diagrams are presented. The CPOs have been measured in plane A and have been rotated 55° clockwise (looking from above) into an equivalent orientation in plane B around an axis perpendicular to the axial plane.

2 and 3 consist of almost pure quartzite layers (total thickness 1–2 cm) which are separated from each other by thin, dark interlayers (Figs. 1b & c). Both samples are parasitic folds from either side of a higher order synform (Fig. 2). The shear fold axis directions vary across the higher order fold by approximately 20°. This variation is probably due to a local fluctuation of the deformation. The axial planes of the folds in sample 2 are greatly deflected around the adjacent fold hinges (Fig. 1b). A lineation runs diagonally across the upper limb and curves around the hinge (Fig. 1d). The orientation of the lineation in the lower limb is parallel to that of the upper limb. The curved lineations define a plane inclined at 35° to the fold axis and perpendicular to the axial plane (plane B, Fig. 3). In sample 3 the orientation of the lineation is of the same type as in sample 2 (Fig. 3), but the plane containing the lineations makes an angle of about 10° with the fold axis. There is no systematic relationship between tightness of the folds and orientation of the fold axis with respect to the lineations.

*Methods of study*

Thin sections were prepared perpendicular to the fold axes in all fold samples (plane A in Fig. 3). Additionally, in samples 2 and 3, thin sections containing the lineation orientations were prepared (plane B, Fig. 3).

Quartz *c*-axes were measured optically with the universal stage at different positions in the hinge and the limbs of the folds in the plane normal to the fold axis. Regions with a homogeneous and representative crystallographic preferred orientation (CPO) were selected using the compensation plate. In such regions all grains (about 250 in each position) were measured on traverses parallel to the axial plane.

The same chips, from which the thin sections had been made, were used as reflection mode samples in the texture goniometer for the *a*-axis determination and slices were prepared from the chips for transmission measurements. All pole figures were orientated with the trace of the axial plane as a horizontal reference line. An average axial plane was approximated for the gently curved axial surfaces of samples 2 and 3.

The image analysis of surface and particle orientations of the quartzites was carried out in sample 1 on thin sections normal to the fold axis and in samples 2 and 3 on thin sections containing the lineation directions (plane B in Fig. 3). Photomicrographs of the quartz microstructures between crossed polarizers were used to trace the grain boundaries. In each fabric, 150 grains were digitized and processed using the SURFOR and PAROR methods outlined in Panozzo (Heilbronner) (1983, 1984) and discussed in the appendix of Schmid *et al.* (1987).

*Optical microstructures*

The quartz in all samples is extensively dynamically recrystallized. Almost all boundaries are quartz–quartz grain boundaries. The boundaries in samples 2 and 3 are bulging and sutured, indicating that some grain-boundary migration had occurred (Figs. 4a & b). However, larger grains also show subgrain formation in samples 2 and 3 (Figs. 4c & d). The angle between the crystallographic orientations of these former subgrains is often more than 15° so that they constitute high-angle boundaries. Some rotation recrystallization boundaries are bulging (Fig. 4d), indicating that grain-boundary migration took place immediately after the formation of new grain boundaries. Thus, it is inferred that subgrain rotation recrystallization and grain-boundary migration occurred simultaneously in these quartzites. Frequently, the rotation recrystallization grain boundaries show a preferred orientation and give the grains a kinked appearance (Figs. 4c & d).

The grain size distribution varies between limbs and hinges. The hinge zones show a bimodal distribution of very small, almost isometric grains (*ca* 0.03 mm in diameter) and large grains up to 0.4 mm long and 0.15 mm across (Fig. 4b). In the limb regions, the grains have a more uniform size of about 0.1 mm (Fig. 4a).

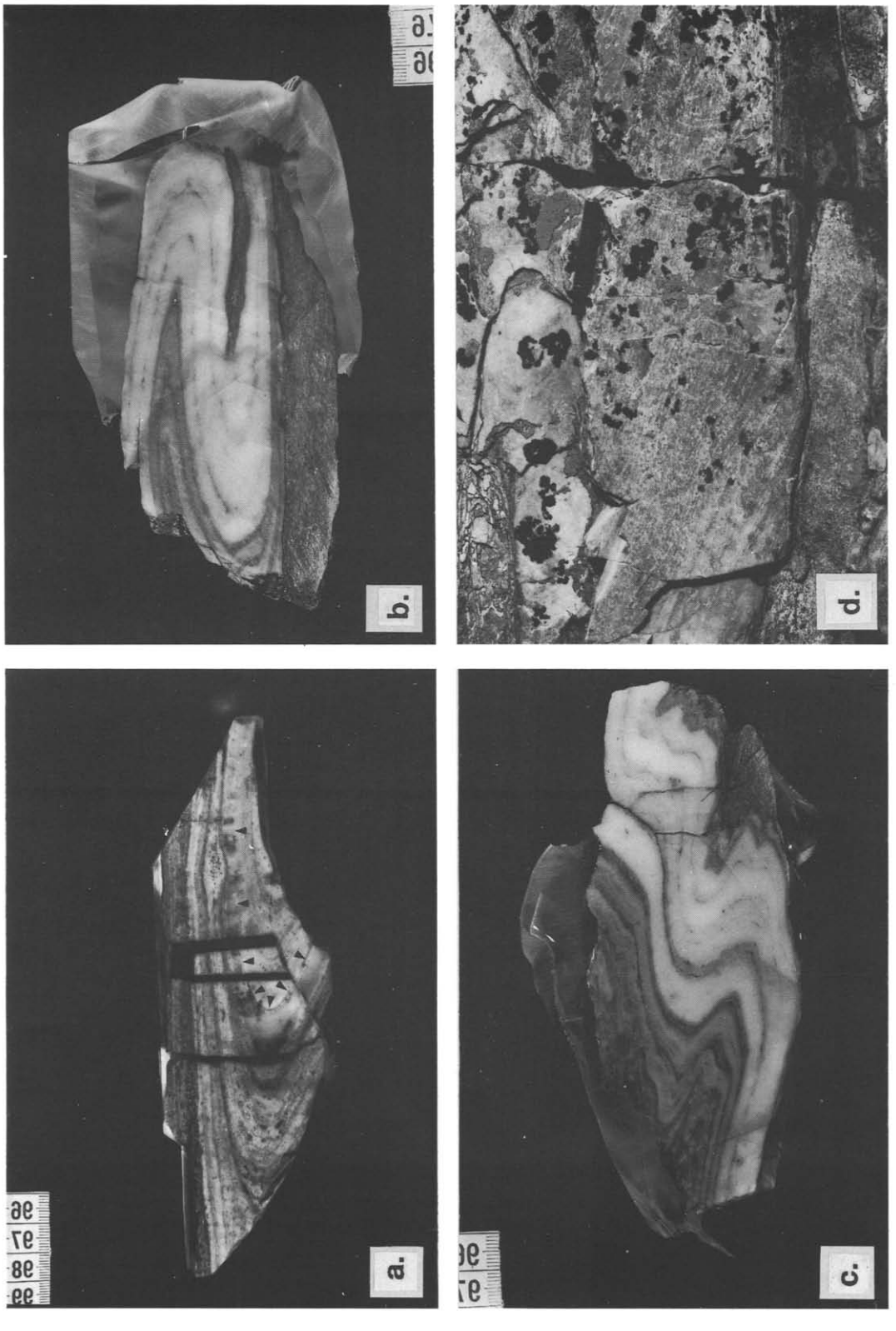


Fig. 1. Photographs of sampled quartzite folds. (a) Quartzite layer (arrows) of sample 1 in a layered albite and zoisite matrix. (b) Isoclinally folded quartzite layers (white) of sample 2 in a paraschist matrix. (c) Quartzite layers of sample 3 in the same paraschist matrix as sample 2. The matrix in samples 2 and 3 consists of quartz + white mica + zoisite ± chlorite. The dark, thin interlayers within the white quartzite bands consist of the same material as the matrix. Folds 2 and 3 are parasitic folds of a higher order fold (see Fig. 2). (d) Lineation across the upper limb of sample 2. View direction is from above. The fold axis is approximately parallel to the bottom margin of the photograph. The curving of the lineation around the fold hinge is weakly apparent.

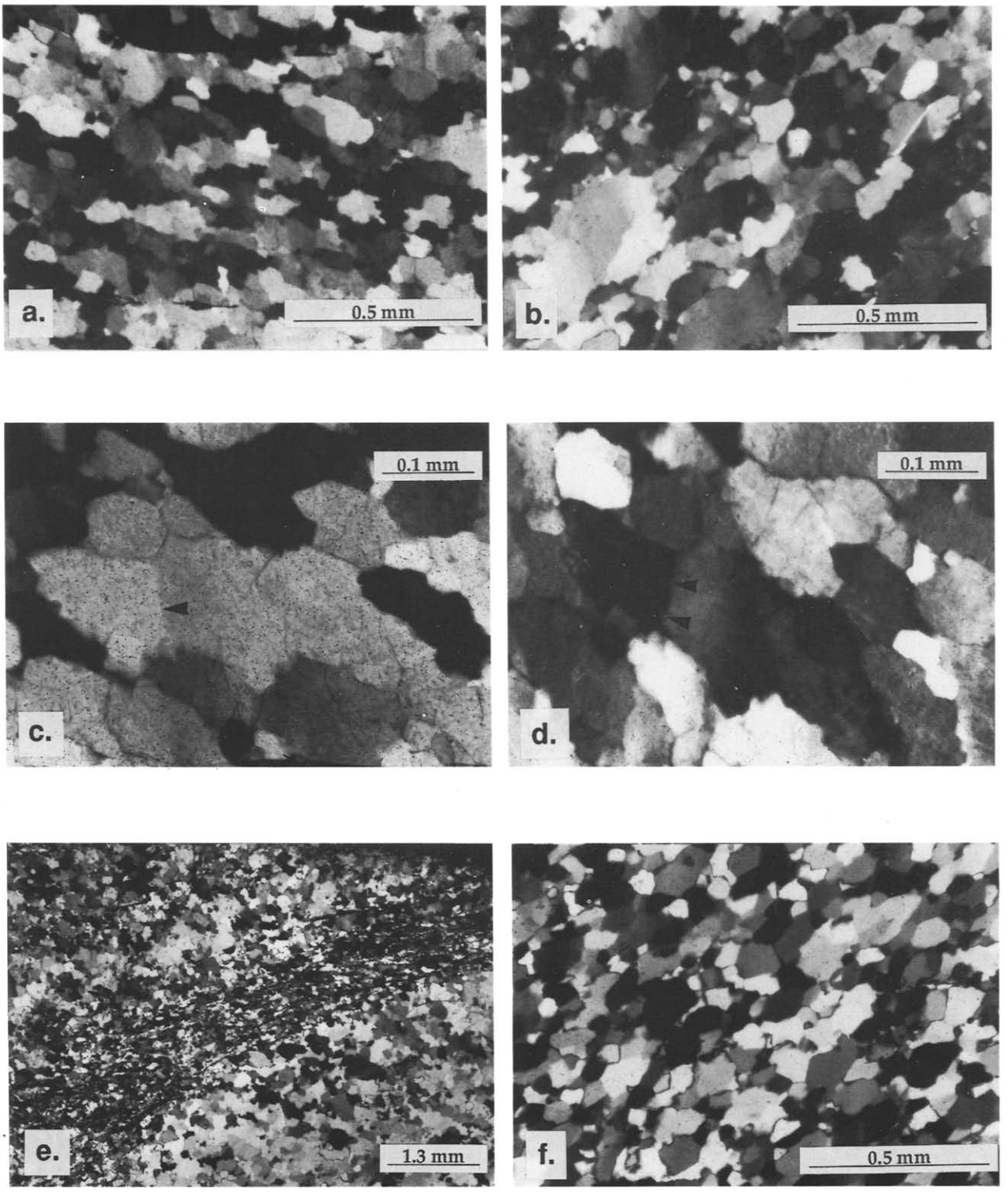


Fig. 4. Quartz microstructures. The axial plane is horizontal in figures (a), (c) & (e). It runs from the bottom left to upper right-hand corner in (b) & (f). (a) The grain boundaries of the limb region in sample 2 show an asymmetric shape fabric and kink-like rotation recrystallization boundaries. The sutured grain boundaries indicate some grain-boundary migration. (b) Quartz microstructure of a hinge region of sample 2. There is a more variable grain size distribution in this microstructure than in (a). As in (a), grain-boundary migration occurred as well as subgrain formation. (c) & (d) Kink-boundary formation due to rotation recrystallization in an elongated quartz grain from a limb region of sample 2. (c) The parent quartz grain, showing a faint grain boundary inside (arrow). (d) The same grain, turned about 20° and displaying the kink boundaries better. Note the weakly bulging kink boundary (arrows), indicating incipient grain-boundary migration of rotation recrystallization boundaries. (e) Quartz grains exhibit smaller grain sizes in a folded inclusion-rich interlayer (quartz + white mica + zoisite ± chlorite) between pure quartzite layers in sample 2. (f) Microstructure in the thicker limb of sample 1. Most quartz grains are elongated and show subgrain boundaries. Weakly lobate grain boundaries indicate some grain-boundary migration.

The inclusion-rich layers, which separate the pure quartzite layers in samples 2 and 3 and mark the folded surface, can have a thickness of up to 1 mm (Fig. 4e). Such thicker inclusion-rich layers consist of quartz + clinozoisite + white mica ± chlorite and have the same composition as the matrix surrounding the pure quartzite layers.

The quartz grains in sample 1 are also elongate (Fig. 4f). The grain boundaries are less sutured than in samples 2 and 3, but show evidence for some grain-boundary migration. Subgrain formation indicates that rotation recrystallization also occurred. The grains have a fairly uniform size, about 0.1 mm across and 0.2 mm in length.

## QUARTZ CRYSTALLOGRAPHIC PREFERRED ORIENTATION (CPO)

The CPOs measured in the plane perpendicular to the fold axis in samples 2 and 3 yield *c*-axis girdles that do not intersect the centre of the pole figure. The *a*-axis girdles have their maximum located off the periphery. Such CPOs suggest that the section perpendicular to the fold axis is oblique to principal kinematic directions. The geometric configuration of the lineations in sample 2 (Figs. 1d and 3) is identical to that of a shear fold (Ramsay 1962, Ramsay & Huber 1987, pp. 482–484). This resemblance to a shear fold suggests that the plane defined by the lineation is a principal kinematic plane containing the shear direction. Therefore, all pole figures of sample 2 have been rotated (clockwise, looking from above) 55°, such that now they are viewed in plane B instead of plane A (Fig. 3). The rotation axis is normal to the axial plane.

The rotated CPOs are shown in Fig. 5. The distribution in all *a*-axis figures determined with the texture goniometer is in good accord with the *c*-axis distributions measured optically. The *a*-axis maximum lies close to the periphery of the diagram and the incomplete *c*-axis single-girdles cross the centre of the pole figures. These features indicate that the orientations of the lineation define a plane containing principal kinematic directions.

The lineation geometry in fold sample 3 is similar to sample 2. However, the azimuth of the lineations differs only about 10° from that of the fold azis. As in sample 2, the pole figures were rotated (80° clockwise around an axis perpendicular to the axial plane, looking from above). The rotated pole figures (Fig. 6) show very similar features to those of sample 2 (Fig. 5).

Fold sample 1 shows single-maxima *c*-axis distri-

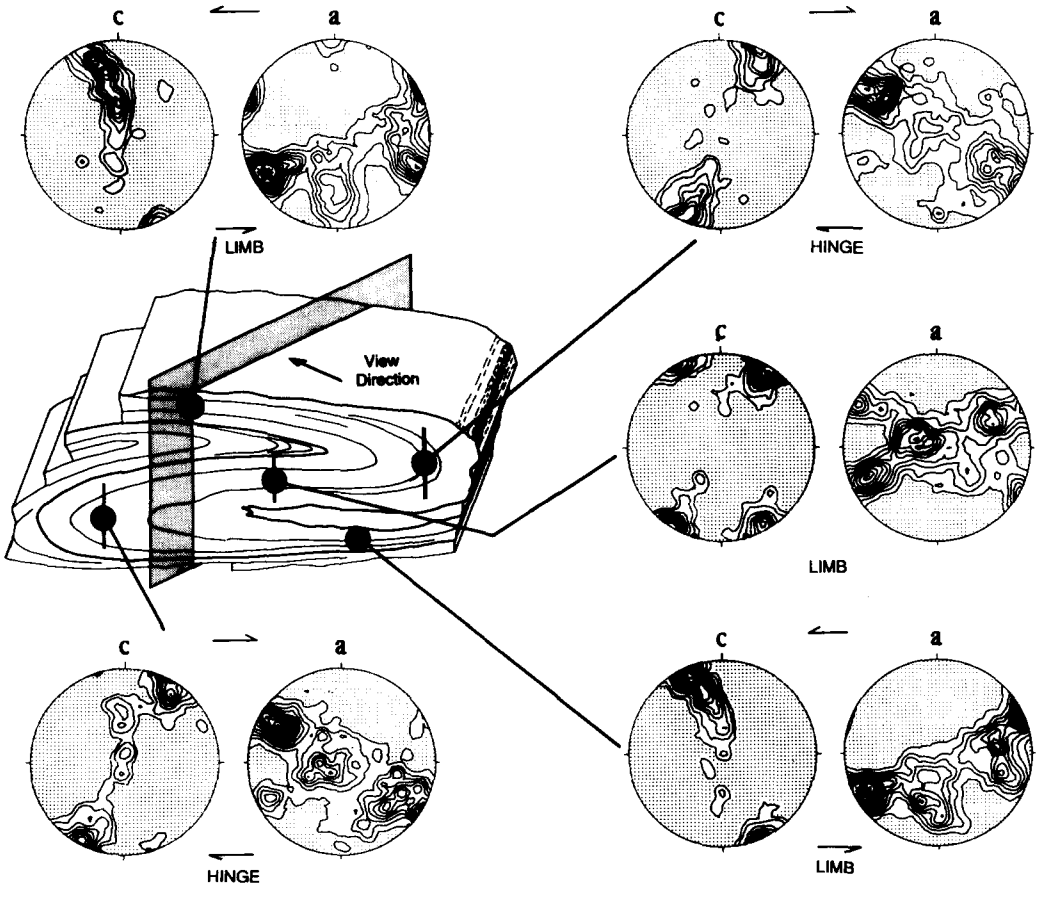


Fig. 5. Quartz *XZ*-CPOs of sample 2, viewed in the plane (shaded), which is defined by the lineation and parallel to plane B in Fig. 3. The inferred shear senses are indicated in the pole figures. *c*-axes of about 250 grains were measured in each location. Lower hemisphere for all pole figures.

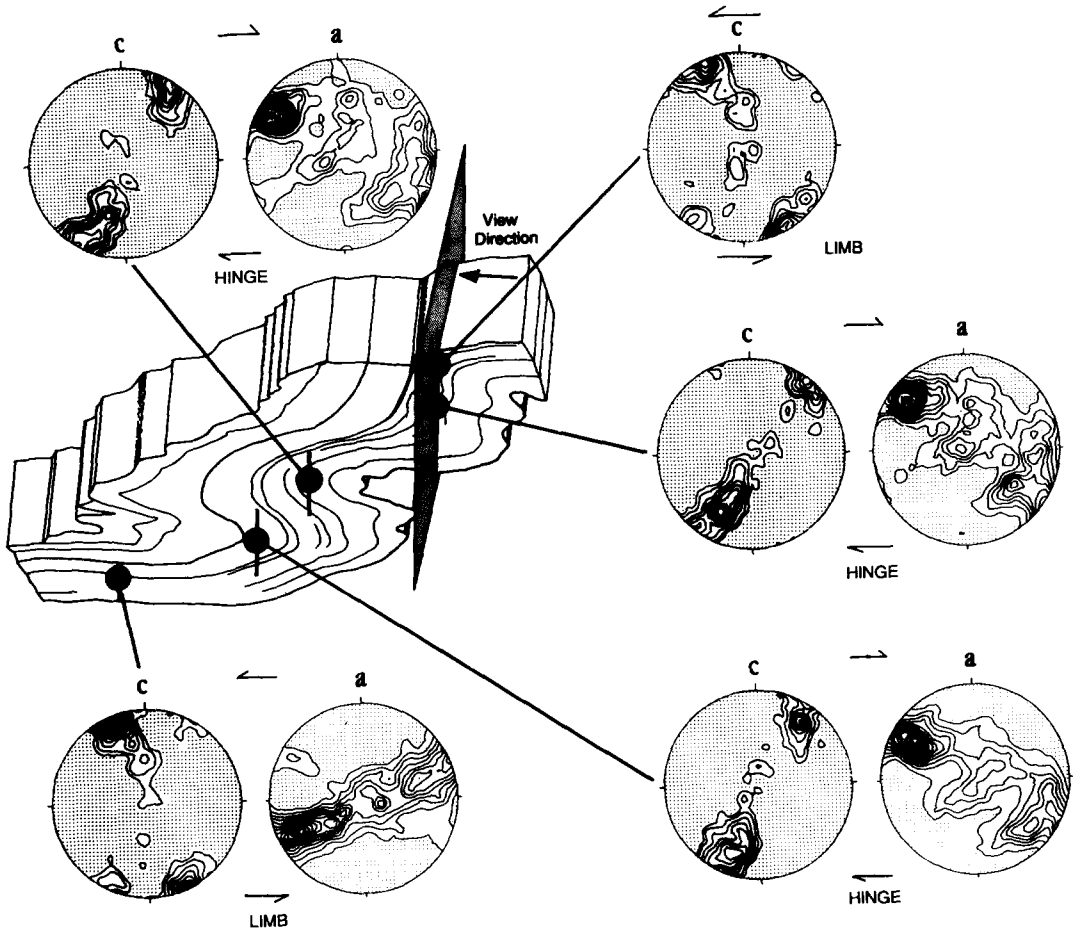


Fig. 6. Quartz *XZ*-CPOs of sample 3, viewed in the plane (shaded), which is defined by the lineation. This plane is inclined to the fold axis at an angle of 10°. Thus, the shear senses indicated are almost parallel to the fold axis. *c*-axes of about 250 grains were measured in each location. Lower hemisphere for all pole figures.

butions in the section perpendicular to the fold axis (Fig. 7). The only *a*-axis pole figure that could be obtained (because of the lack of homogeneous quartzite material in the thin limb) shows a single-girdle with a maximum near the periphery of the diagram (Fig. 7). The CPOs suggest that the section normal to the fold axis and lineation contains the principal kinematic directions.

*Discussion of the quartz CPO*

*Samples* 2 *and* 3. The symmetry of the *c*- and *a*-axis pole figures is monoclinic and thus indicative of rotational, non-coaxial deformation (Bouchez & Pêcher 1981, Garcia Celma 1983, Law *et al.* 1986, Schmid & Casey 1986). The sense of shear during the rotational deformation can be determined from the CPOs in quartz (Simpson & Schmid 1983, Lister & Snoke 1984, Law *et al.* 1986, Schmid & Casey 1986). As pointed out above, the shear senses refer only to the individual folds in which they are determined. The obliquity of the CPO is mirror-symmetric in limbs and hinges, indicating a sinistral shear sense in the fold limbs and a dextral one in the hinge regions. One important aspect of the shear directions is that they all lie in a plane, which is defined by the lineation and is oblique or subparallel to the fold axis (Figs. 3, 5 and 6). The CPO of the inner limb in sample 2 (Fig. 5) differs from the others in that it has orthorhombic symmetry. The CPO is analogous to the quartz CPOs found in fold hinges (Hara 1971) or obtained from coaxial deformation experiments (Dell'Angelo & Tullis 1986). The orthorhombic symmetry and analogies with coaxial deformation settings are consistent with a coaxial plane strain deformation (Hara 1971, Schmid & Casey 1986). Consequently, the intermediate *Y*-axis of the finite strain ellipsoid of the inner limb in sample 2 (Fig. 5) lies perpendicular to the plane B, defined by the lineation (compare Fig. 3). The shortening direction of the coaxial plane strain deformation is perpendicular to the axial plane.

Thus, not only those CPOs that indicate rotational deformation, but also those that reflect coaxial plane strain deformation lie in the same plane in samples 2 and 3. This plane is always perpendicular to the axial plane and contains the observed lineation; it is independent of the sense of shear in the different parts of the fold, of the fold axis orientation, and of coaxial or non-coaxial deformation. The concentration of *c*-axes in a single maximum suggests a predominance of basal glide (Lister & Dornsiepen 1980, Schmid & Casey 1986).

*Sample* 1. The oblique single-maximum distribution of *c*-axes and the *a*-axis maximum near the periphery in

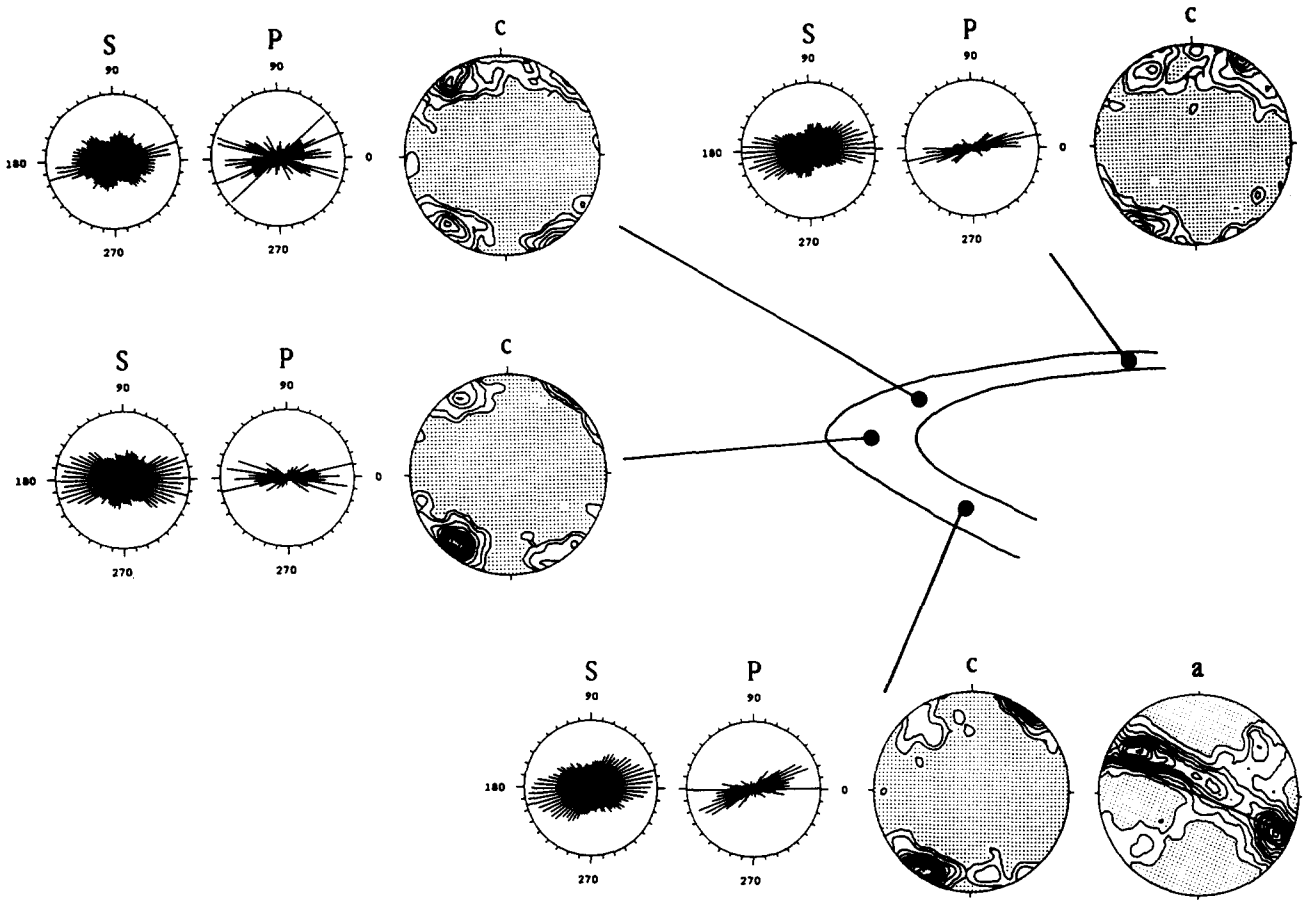


Fig. 7. Quartz *XZ*-CPOs and shape fabric diagrams in sample 1, shown in the section perpendicular to the fold axis. Surface ODF = S, Particle ODF = P. 150 grain outlines were digitized for each shape fabric. *c*-axes of about 250 grains were measured in each location. Lower hemisphere for all pole figures.

the bottom limb of sample 1 (Fig. 7) indicate a rotational deformation with dextral shear sense. The section in Fig. 7 is perpendicular to the fold axis and contains the shear direction in this fold. The thinner limb of sample 1 shows *c*-axis distributions similar to those in the inner limb of sample 2 (Figs. 5 and 7). Thus, a component of coaxial plane strain deformation is inferred, such that in sample 1 the intermediate *Y*-axis of the finite strain ellipsoid coincides with the direction of the fold axis. The coaxial shortening direction is almost normal to the axial plane. The hinge region prepresents an intermediate pattern between predominantly coaxial and rotational deformation types. The absolute positions of the *c*-axis maxima do not change around the fold hinge; only the relative intensities of rotational and simple shear deformation vary around the fold in sample 1. However, the shear sense and the orientation of the *XZ* plane of the finite strain ellipsoid remain constant.

## SHAPE FABRICS

To investigate the differences between the microstructures in limbs and hinges in more detail, the grain boundaries in the lineation planes in samples 2 and 3 and in the plane normal to the fold axis in sample 1 have been analysed using the SURFOR and PAROR method of Panozzo (1983, 1984). The surface and particle ODFs (orientation distribution functions), which are analogous to orientation histograms, are presented in Figs.8–10.

### *Samples 2 and 3*

The surface and particle ODFs indicate a clear distinction between limb and hinge shape fabrics on the basis of the sense of the inclination with respect to the axial plane and the different internal symmetries of the shape fabrics. The maxima of the limb surface and particle ODFs are 10–30° clockwise with respect to the horizontal (axial plane), whereas in the hinges they are 10–30° counterclockwise with respect to the horizontal (Figs. 8 and 9). It is easier to compare the different symmetries of limbs and hinges in an orthogonal plot of the surface ODF (Fig. 10). The angles of the rose diagrams in Figs. 8 and 9 are plotted on the *x*-axis and the relative length of line segments on the *y*-axis. There is a lack of mirror-symmetry in the limb surface ODFs arising from a plateau or a submaximum about 50° from the maximum (Figs. 10 a–c). The ratio between maximum and minimum of the limb surface ODFs is about 0.6, whereas that of the hinges is about 0.4 (Figs. 10c & f); it follows that generally the limb patterns are more anisotropic than the hinge patterns.

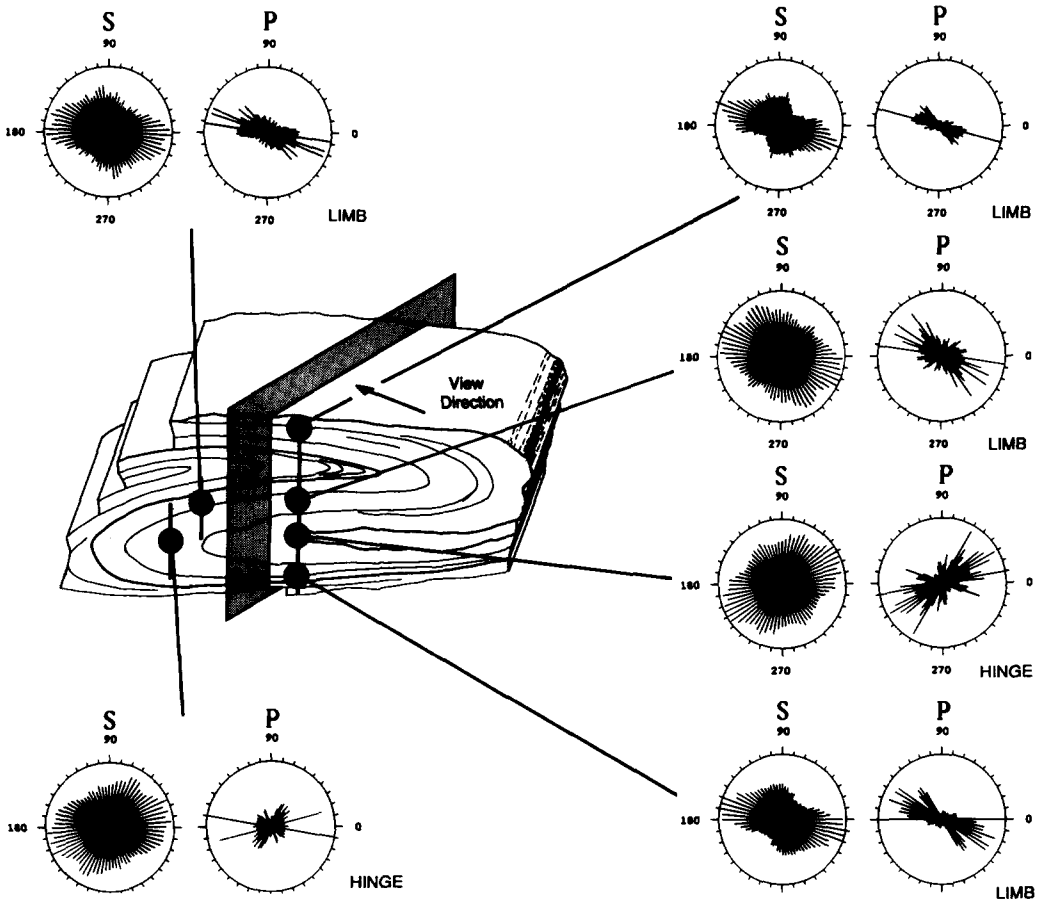


Fig. 8. Shape fabrics of sample 2. All shape fabrics were digitized in the section (shaded) defined by the lineation orientations (compare Fig. 3). Hinge and limb regions show opposite shear senses. Surface ODF = S, Particle ODF = P. 150 grain outlines were digitized for each shape fabric.

The surface ODFs are very sensitive to changes in the microstructure: in the middle fold hinge in Fig. 9, three microstructures were digitized immediately adjacent to each other, so that the changes between hinge and limb microstructures are recorded. The intermediate surface ODF is inclined to the right like those of the limbs (consistent with an oblique sinistral CPO), but shows the mirror-symmetric and more isotropic characteristics of the hinges. Similarly, the symmetry of the surface ODF of the inner limb in sample 2 (Fig. 8) resembles hinge regions, but is inclined to the right like other limb ODFs. Thus, the changes in inclination sense in the surface ODFs are abrupt and are consistent with those of the CPOs, whereas the symmetry characteristics of the microstructure adjust more progressively.

The particle ODFs, i.e. the ODFs of long axes, do not produce smooth diagrams like the surface orientations. This is mainly due to statistics: the surface ODF represents 13,000–15,000 line segments, whereas there are only about 150 grains (=particles) per fabric. However, the particle ODFs of the limbs show a maximum sector which has a similar orientation as the maximum of the surface ODFs (Figs. 8 and 9). The particle ODFs of the limbs display a sharp decrease from the maximum to the minimum, i.e. the particles show a strong alignment of their long axes. Conversely, the particle ODF maximum sectors in the hinges are less well defined and usually do not coincide with the surface maximum sector, so that the orientation of the long axes of the grains varies and is different from the surface distribution.

*Sample* 1

The surface OFDs in fold sample 1 in the section perpendicular to the fold axis show no significant difference between limb and hinge regions (Fig. 7). The surface fabrics are strongly anistropic, which indicates a directional alignment of the grain boundaries. The maxima are always at a small angle counterclockwise from the horizontal (axial plane). The surface ODFs are mirror-symmetric (bottom limb) or almost mirror-symmetric internally (upper limb). However, the slight differences in symmetry are not consistent or systematic throughout the fold (Fig. 7). The maximum sector of the anisotropic particle ODFs coincides with the maximum of the surface fabrics.

## DISCUSSION OF THE SHAPE FABRICS

*Samples* 2 *and* 3

Oblique shape fabrics in quartzites from rotational deformation regimes have been described in the litera-

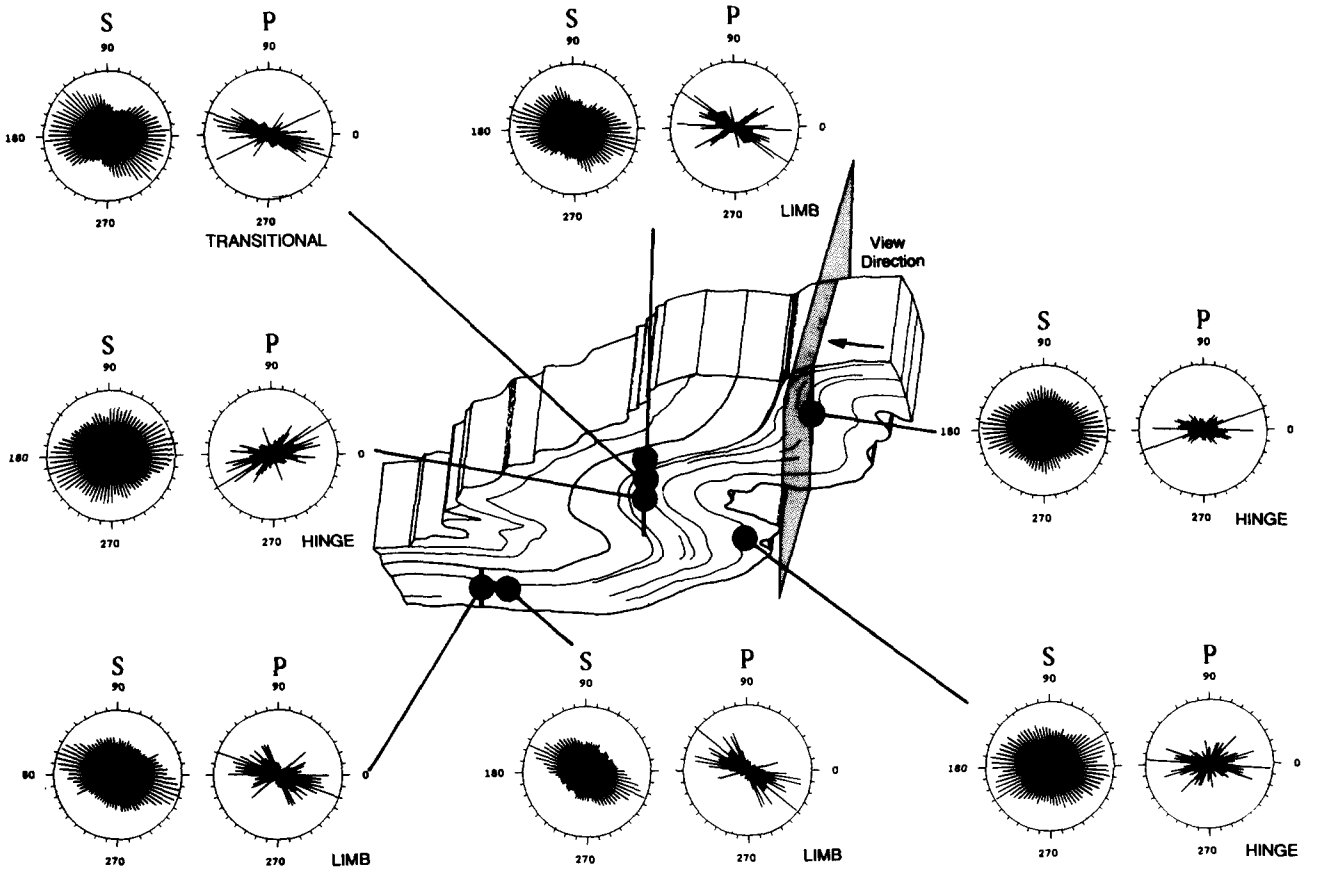


Fig. 9. Shape fabrics of sample 3. All shape fabrics were digitized in the section (shaded) defined by the lineation orientations. Hinge and limb regions show opposite shear senses. Surface ODF = S, Particle ODF = P. 150 grain outlines were digitized for each shape fabric.

ture (Garcia Celma 1982, Lister & Snoke 1984, Burg 1986, Law *et al.* 1986, Knipe & Law 1987) and are reliable shear sense criteria, as shown by Brunel (1980), Simpson & Schmid (1983) and Lister & Snoke (1984). The sinistral shear sense in the limb regions, which has been deduced from the CPOs is consistent with the clockwise rotation of the surface and particle ODFs with respect to the horizontal (axial plane). The same agreement between CPOs, surface and particle ODFs and dextral shear sense is found in the hinge regions.

The shape fabrics do not result from a passive rotation of grain boundaries because rotation recrystallization and some grain-boundary migration have occurred in these quartzites. Thus, the development of the shape fabrics is not a strain feature (Means 1981, Hanmer 1984) and has to be evaluated in conjunction with the deformation mechanisms and the CPO (Schmid *et al.* 1987). These features will be discussed below.

The maxima in the surface and particle ODFs reflect the grain elongation, which is consistent with the plastic deformation of the grains (Means 1981, Lister & Snoke 1984). The submaxima in the limb surface ODFs probably reflect the influence of rotation recrystallization: the optical microstructures in the limb regions show rotation recrystallization with a kink-like appearance of the grains. The kink boundaries have a preferred orientation that lies at an angle of approximately 70–75° to the axial plane (rotated clockwise with respect to the horizontal; Fig. 11). This orientation coincides with that of the submaximum of the surface ODFs. Thus, the asymmetric limb surface ODFs reflect the preferred orientation of the kink boundaries and a predominance of rotation recrystallization in the limbs (Figs. 4a,c & d, 8, 9 and 10).

In addition to rotation recrystallization, some grain-boundary migration occurred in these quartz microstructures (Figs. 4a–d). The surface and particle ODFs of the hinges are consistent with a greater contribution of grain-boundary migration: initially straight grain boundaries become progressively more corrugated during grain-boundary migration (Means 1983, Urai 1983, Jessel 1986, Wilson 1986, Urai *et al.* 1986). The greater corrugation of grain boundaries yields a lower anisotropy of the grain boundary (=surface) ODF and a weaker correspondence of surface and particle ODF in the hinge regions (Figs. 8–10). The observed bimodal grain size distribution in the hinge regions supports this interpretation, because during grain-boundary migration the variation in grain sizes increases, while the mean grain size remains fairly constant (Means 1983).

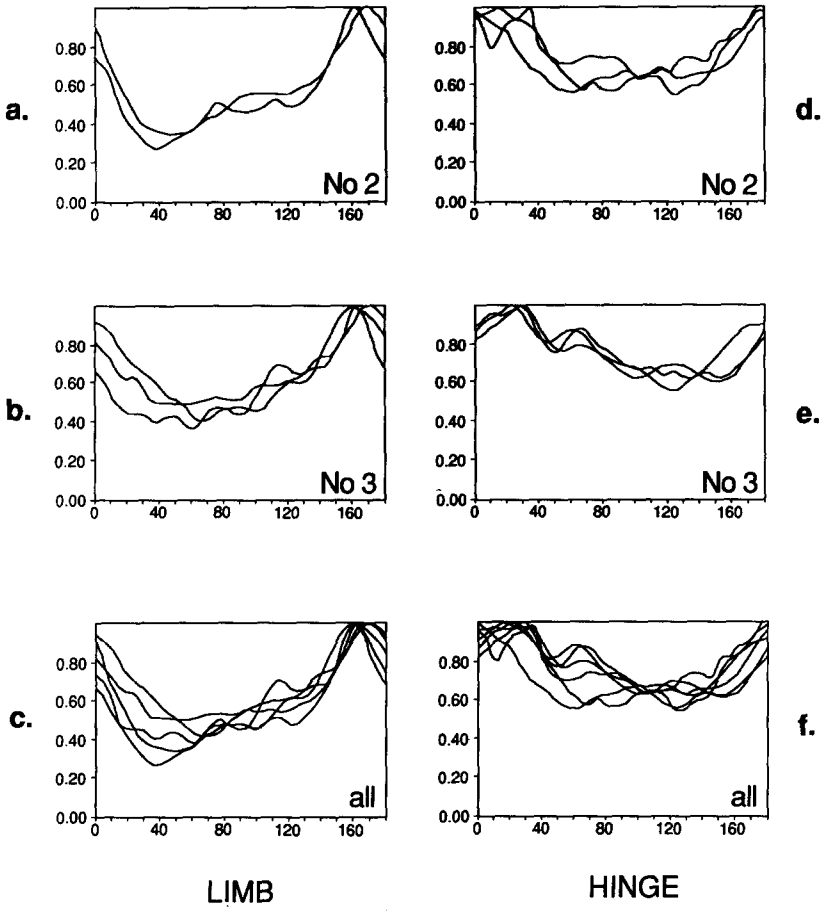


Fig. 10. Surface ODFs in orthogonal diagrams. $x$-axis = angular orientation with respect to the reference line (axial trace), $y$-axis = line segment length divided by the longest. (a) Limb surface ODFs of sample 2; (b) limb surface ODFs of sample 3; (c) all limb surface ODFs; (d) hinge surface ODFs of sample 2; (e) hinge surface ODFs of sample 3; (f) all hinge surface ODFs.

Thus, the differences in the symmetry and anisotropy of the surface ODFs in limbs and hinges can be interpreted in terms of differences in the microstructural development. The limb microstructures are characterized by a predominance of rotation recrystallization which 'resets' the microstructure by the generation of new grains after the grains have been elongated through plastic deformation (Means 1981, Lister & Snoke 1984).

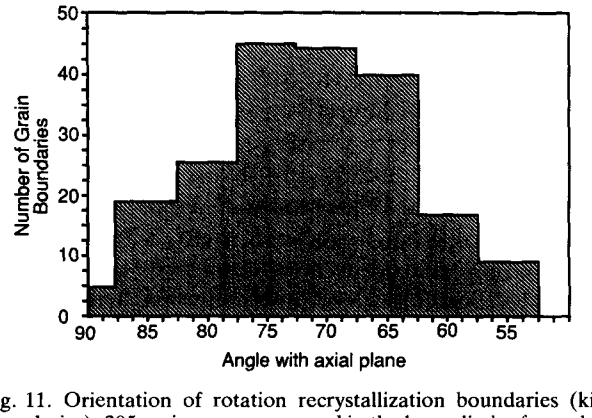


Fig. 11. Orientation of rotation recrystallization boundaries (kink boundaries). 205 grains were measured in the lower limb of sample 3. The angle with respect to the axial plane refers to a clockwise rotation with respect to the horizontal (axial plane). The boundaries show a preferred orientation with a maximum near 70–75° to the axial plane.

The contribution of rotation recrystallization to the formation of new grains is smaller in the hinges, so that the microstructure reflects a greater influence of grain-boundary migration than in the limbs.

*Sample* 1

The surface ODFs of sample 1 (Fig. 7) are quite different from samples 2 and 3. No submaxima are present and limb and hinge regions do not differ much from each other. Only the intermediate pattern between limb and hinge positions is different from the others. The reason for the different surface ODF in the intermediate hinge/limb position is not clear.

It is interesting to note that the surface ODFs are invariant with respect to the differences in the CPOs (Fig. 7). For example, the predominantly coaxially deformed quartzite in the thinner limb produces a similar, inclined surface and particle ODF as in the predominantly rotationally deformed lower limb. This observation is consistent with the fact that the surface ODFs change their symmetry less abruptly than their shear sense characteristics which always coincide with the CPO. The difference is probably due to the fact that the surface ODF reflects the recrystallization mechanism better than the CPO.

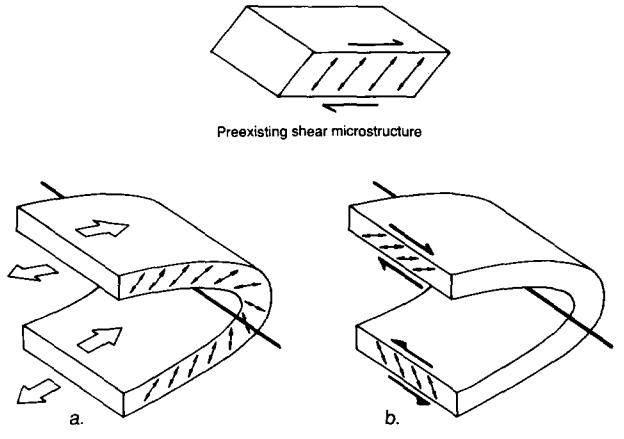


Fig. 12. Schematic diagram, showing the geometry of a pre-existing CPO or microstructure, which is passively rotated by later folding. (a) Fold axis perpendicular to the pre-existing shear direction. The shear sense remains the same in the limbs. (b) Fold axis parallel to the pre-existing shear direction. The shear sense is opposite in both limbs.

## DISCUSSION OF THE FOLDING DEFORMATION

### *Relative timing of shear deformation and folding*

The timing relationships between folding and shearing can be established in all samples.

Consider two different sequences: (a) first shearing and then folding; and (b) first folding and then shearing. If the shear microstructure pre-dates folding and the shear direction is orientated at a large angle to the fold axis, the resulting shear senses are the same in both fold limbs, but different in the hinge (considering a passive rotation of the limbs; Fig. 12a). If the folding does not rotate the limbs passively but involves flexural-slip or shear folding, the resulting shear couples in the limbs are opposite to each other. The shear direction in sample 1 is approximately perpendicular to the fold axis. No CPOs indicating different shear senses and no different hinge CPOs have been found in sample 1 (Fig. 7). Therefore it can be concluded that the simple shear CPOs and shape fabrics were not modified by a later folding event. Similar CPOs indicating a constant shear sense were found in isoclinal folds by Carreras *et al.* (1977) and Price (1981). In case (b), if shear deformation had taken place after folding, it would have to be a localized, heterogeneous shear deformation, because the thinner limb (Fig. 7) does not show simple shear CPOs. A localized dextral shear deformation in the hinge and thicker limb is not consistent with the fold shape. It is therefore concluded that folding and simple shear deformation occurred approximately at the same time.

In samples 2 and 3, a rotation of the simple shear CPOs and shape fabrics by later folding can also be excluded: in samples 2 and 3 the shear sense is sinistral in all limbs of the parasitic folds of the higher order fold (Figs. 2, 5 and 6). The shear direction is almost parallel to the fold axis (sample 3) or inclined to it (sample 2). If the fold axis is inclined at a small angle to an earlier shear direction, the pre-existing shear direction is reversed in one limb (considering a passive rotation of the limbs, Fig. 12b). If the folding involved flexural-slip or shear folding, the shear couples in the limbs will also be opposite. Thus, the same shear sense in the limbs of parasitic folds on either side of the major fold (Fig. 2) excludes a rotation of the limbs after a shear deformation. If shear deformation had occurred after folding, the shear senses in the hinges, which are opposite to the other fabrics, could only be explained as domains which were unaffected by this later shear deformation, i.e. representing relict domains. Although this interpretation is probably correct to some degree (it will be pursued below), it should be emphasized that in both samples 2 and 3, the hinge and limb CPOs lie in the same plane. Such a coincidence in orientation of shear CPOs and older relict CPOs appears improbable, unless the shear deformation and folding occurred *approximately* at the same time.

The fold shapes of sample 2 indicate that the behaviour of the hinges differs from that of the limbs during the late stages of the deformation: the inner limb and hinges are thicker than the outer limbs and the axial planes gently curve around the adjacent fold hinge. These two features can either be explained by a late flattening of the fold normal to the axial plane or by a simple shear deformation, which takes place preferentially in the outer limbs. The late flattening of the fold is unlikely because only simple shear CPOs have been found in the outer limbs. Thus, it is more likely that the hinges and the inner limb in sample 2 have not been deformed (or only at lower strain rates) during the last stages of the shear deformation, which caused the thinning and a weak anastomosing of the outer limbs around the hinges. This explanation implies that the hinges and inner limb in sample 2 represent relict or 'retarded' microstructures during the last stages of the deformation.

A prevalence of simple shear deformation in the outer limbs during the last deformation stages is consistent with the rotation recrystallization of quartz, thus 'resetting' of the microstructures occurs. If the hinges do not deform extensively during the last deformation stages, rotation recrystallization should be of minor importance. Some grain-boundary migration, however, is likely to prevail and would produce a greater tendency towards annealed microstructures in the hinges. This interpretation agrees well with the observed differences in the shape fabrics in limbs and hinges of samples 2 and 3.

It is not clear why the hinges may have ceased to deform during the late stages of the shear deformation. One possibility is that the mechanical properties of the quartzite change due to a reorientation of the CPO and shape fabrics during folding. In other words, the acquired shape fabric and CPO represent a configuration in equilibrium with the deformation conditions and if this configuration is changed by rotation of the fabric and the CPO with respect to the kinematic direction (bending of layers in the hinge), it might cause a relative hardening and a different development of the CPO of the rotated material. Ralser (1987) found a

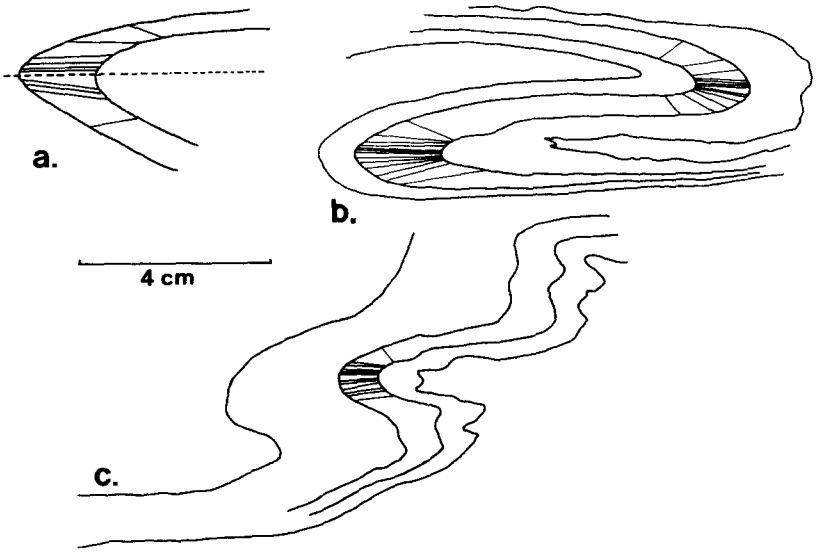


Fig. 13. Dip isogons of the investigated fold samples. (a) Sample 1, showing a type 3 fold geometry. (b) Sample 2, showing a type 1c fold geometry. (c) Sample 3, also showing a type 1c fold geometry.

strength difference of 200–400 MPa and a different development of the CPO in experimentally deformed quartz mylonites, depending on the orientation of the pre-existing CPO with respect to the shortening direction. However, it is difficult to apply the results of his coaxial experiments to the shear deformation environment found in these samples.

*Kinematic relationship between shear deformation and folding process*

The conclusion drawn above that folding and shear deformation occurred approximately at the same time, together with the geometry of the folded lineation (Fig. 1d), suggest that the folds originated by shearing. Heterogeneous simple shear for the formation of perfect similar folds has been suggested as the only mechanism that explains the geometry of perfect similar folds (Ramsay 1967, pp. 429–436). The dip isogons of the folds have been constructed for the section normal to the fold axis in order to analyse the accurate fold geometries (Fig. 13).

Fold 1 is a type 3 fold, whereas folds 2 and 3 are type 1c folds (Ramsay 1967, pp. 365–370). Since the folds do not display perfect similar geometries, buckling components probably played a role in their formation. The different fold types in samples 1, and 2 and 3 indicate an opposite competence relationship between the quartzite layers and matrix in sample 1 vs 2 and 3. The opposite competence relationship could perhaps explain why in samples 2 and 3 the limb and hinge CPOs and shape fabrics differ, whereas in sample 1 they do not. However, it remains unclear, why the shear senses in limbs and hinges in samples 2 and 3 are opposite to each other. The buckling components will be considered below.

The thin interlayers between the pure quartzite layers (sample 2, Fig. 4e) have been found to show a quartz CPO different from that of the pure quartzite layers (Fig. 14). The interlayer CPOs are presented in the same orientation as the CPOs from the pure quartzite layers, i.e. rotated into the plane containing the lineation and general shear direction (see Fig. 3). The interlayer CPOs consist of a more complete skeleton of a type 1 crossed-girdle than the pure quartzite layers. Opposite shear

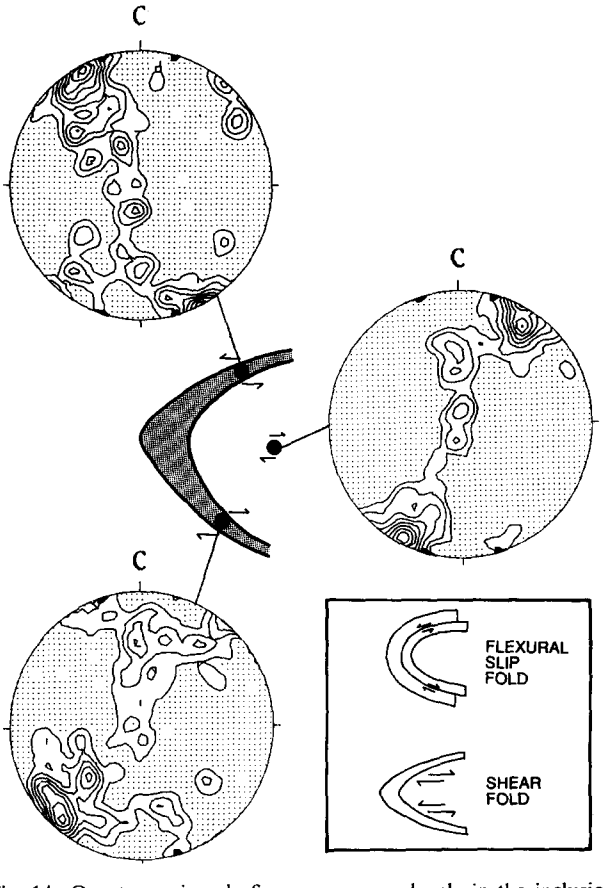


Fig. 14. Quartz *c*-axis pole figures, measured only in the inclusion-rich interlayer (shaded) in the left one of the two hinges of sample 2. Pole figure in the centre is from the pure quartzite layer for comparison. The upper diagram represents 156 grains, the lower diagram 205 grains, lower hemisphere in all pole figures. All CPOs are presented in the same plane (defined by the lineation) as the other quartzite pole figures in Fig. 5 (see also Fig. 3).

senses can be concluded from the CPOs on either side of the fold hinge. The inset in Fig. 14 shows that the shear senses are opposite to those required for a shear fold. The shear senses in the interlayers are best explained as having been formed by flexural-slip during buckling of the layers (see inset of Fig. 14). The inclusion-rich interlayers consist of the same material as the matrix around the quartzite layers. The fold type 1c deduced from the dip isogons of the pure quartzite layers (Fig. 13) indicates that the surrounding matrix is less competent than the pure quartzites. The less competent material in the interlayers thus accommodates the buckling of the more competent layers by flexural-slip (Fig. 14). The interlayer CPOs have their principal kinematic directions in the same plane as the pure quartzite CPOs. This orientation of the interlayer quartz CPOs implies that the flexural-slip vector during the buckling of the layers is contained in the same plane as the shear deformation in the pure quartzite layers. Since this plane is inclined to the fold axis, it can be concluded that the flexural-slip accommodating the buckling of the pure quartzite layers occurred oblique to the fold axis ('oblique flexural-slip fold' or 'oblique flow buckle fold', Ramsay 1967, p. 395, Ramsay & Huber 1987, p. 489).

The question whether the flexural-slip CPOs record the initiation or the last stages of the flexural-slip is critical for the interpretation of the orientation and possible rotation of the fold axis with respect to the shear direction. If the CPOs record the initiation of the fold, the fold axis remained in a stable position with respect to the shear direction. If only the last flexural-slip movements are recorded, the fold axis may have rotated towards the shear direction since the fold initiation. The finite shear strain in the interlayer portions, where the CPOs have been measured (Fig. 14), is between $\gamma = 2$ and $\gamma = 2.5$ (using the same arc length of the two interlayer boundaries, measured from the hinge). The interlayer is thinned towards the limbs, so that these $\gamma$-values represent maximum values. Experimental simple shear deformation of quartzites shows that a type 1 crossed-girdle *c*-axis CPO develops during dislocation creep after a finite shear strain of about $\gamma = 1.3$–2, whereas single-girdle CPOs require shear strains of $\gamma > 2$ (Dell'Angelo & Tullis 1989). The CPO of the interlayer represents an intermediate stage between a crossed- and single-girdle (Fig. 14), so that a shear strain of approximately $\gamma = 2$ appears to be a reasonable estimate for the minimum shear strain required to produce such a CPO. Taking all these numbers as crude estimates, it is inferred that the interlayer CPOs record almost all of the total flexural-slip shear strain. Thus, the flexural-slip vector must have maintained its present orientation with respect to the fold axis during a large part of the flexural-slip folding. Therefore, the fold axis probably did not rotate much since its initiation. The fact that the geometry of the CPOs in sample 3 is identical to that in sample 2 (except for the interlayers, which could not be measured), suggest a similar lack of rotation of the fold axis with respect to the shear direction.

The inner limb in sample 2 indicating coaxial plane strain has the *Y*-axis inclined to the fold axis. The *XZ* plane of the finite strain ellipsoid has the same orientation as that of the simple shear deformation of all other CPOs. This geometry agrees with the conclusion drawn from the interlayer CPOs that the fold axis was oblique to the shear direction during a large part of the folding.

The apparently stable orientation of the fold axis with respect to the shear direction during a shear strain of the order of $\gamma = 2$ is not in accord with the widely established concept of simple shear deformation of folds and the numerous examples of rotated fold axes (e.g. Sanderson 1973, Escher & Watterson 1974, Bak *et al.* 1975, Rhodes & Gayer 1977). This unusual behaviour is difficult to explain. One possible explanation might be a strain partitioning between the fold hinges and the limbs. The 'retarded' microstructures in the fold hinges suggest a strain partitioning, at least for the last deformation increments. Another tentative explanation might be that the folds, once formed, may represent a mechanical linear anisotropy, e.g. the hinges of the parasitic folds themselves or the quartz shape fabrics (Cobbold & Watkinson 1981, Watkinson & Cobbold 1981), and thus develop a resistance to a modification of their structure (Ghosh & Ramberg 1968, Skjernaa 1975, Watkinson 1981). Hence, the folds could represent configurations which are difficult to modify by the shear deformation for mechanical reasons. This hypothesis is supported by the fact that in sheath folds the reorientation of fold axes is inferred to take place by kinematic amplification of passive boundary layers (Cobbold & Quinquis 1980, Berthé & Brun 1980), whereas the layers in samples 2 and 3 have been mechanically active throughout their deformation history.

### *Origin and character of the observed lineations*

The results from the CPO and shape fabric analysis suggest that the lineations in the samples were produced by different mechanisms.

The lineation in sample 1 is parallel to the fold axis. Given the presence of crenulated inclusion-rich layers, the lineation is most likely produced by these crenulations. In any case, the orientation of the CPOs indicate a shear direction perpendicular to the lineation and demonstrate that the lineation in sample 1 is not a stretching lineation.

The lineations in samples 2 and 3 represent stretching lineations because the plane of the lineation exactly contains the shear direction. The conclusion that buckling and shear deformation took place in the same plane, explains that the stretching lineation curves around the hinge in sample 2. Since the buckling (i.e. rotation axis) is perpendicular to the shear direction (despite the oblique orientation of the fold axis) the curved stretching lineation lies in a plane.

It is interesting to note that the crenulation lineation of sample 1 and the stretching lineations of samples 2 and 3 cannot be distinguished in the field by appearance. Thus, it should be emphasized that the character of a lineation has to be determined by a microstructural or,

better, a CPO study and cannot be assessed from geometrical relationships, e.g. within a fold.

## CONCLUSIONS: MODELS FOR FOLDING AND SHEAR DEFORMATION

In order to explain the observed geometries and kinematics of the samples, models for the development of the folds are proposed. The models are designed to explain the following aspects, which can be inferred from the geometric and kinematic analysis of the folds.

(1) The principal kinematic directions lie in a single plane for all parts of each individual fold. This is the case for simple shear and coaxial deformation components.

(2) The plane containing the principal kinematic directions (the $XZ$ plane of the finite strain ellipsoid) in samples 2 and 3 is defined by the lineations, which are therefore stretching lineations. The orientation of the lineation in sample 1 is perpendicular to this plane and is therefore not a stretching lineation.

(3) The $XZ$ plane of the finite strain ellipsoid is oblique to the fold axis and normal to the axial plane in samples 2 and 3, whereas it is normal to the fold axis in sample 1.

(4) In folds 2 and 3 buckling is concluded to be the folding mechanism. The flexural-slip vector in the interlayers lies in the same $XZ$ plane as the simple shear and coaxial plane strain deformation (in sample 2). It is very unlikely that substantial rotation of the fold axis towards the shear direction has occurred in sample 2.

(5) The hinges of samples 2 and 3 are interpreted as relict or 'retarded' structures during the last deformation increments. The difference between shape fabrics in hinges and limbs are explained by more abundant rotation recrystallization in the limbs than in the hinges.

(6) Shear deformation and folding take place approximately simultaneously in all samples, but the simple shear deformation continues in the limbs after the deformation ceased in the hinges (samples 2 and 3).

Theories for folds in simple shear deformation have been developed (e.g. Ramsay 1960, 1962) and such folds have been modelled (Casey & Huggenberger 1985, Manz & Wickham 1978). In all of these models the deformation is simple shear or simple shear combined with homogeneous pure shear. Although it is possible for such folds to have their axes perpendicular to the shear direction, the general case is represented by folds whose axes are oblique to the shear direction (Ramsay 1962). In the latter case, the layer boundaries are mechanically passive markers. Since in all samples the folding involved mechanically active layers, somewhat different models for the folding and shear deformation have to be developed to explain the conclusions drawn above. Especially, the apparent lack of rotation of fold axes towards the shear direction, deduced from CPOs and absence of curved fold axes in the field, have to be accounted for.

As a first possibility, a model is considered (Fig. 15a), where the anisotropy lies in the $XZ$ plane during simple shear (Escher & Watterson 1974). Simple shear, which may be combined with components of coaxial deformation, folds the anisotropy planes and causes a shear deformation of the whole block (Fig. 15a). The fold axes in this case are expected to lie parallel to the extension direction, and the axial plane is parallel to the $XY$ plane

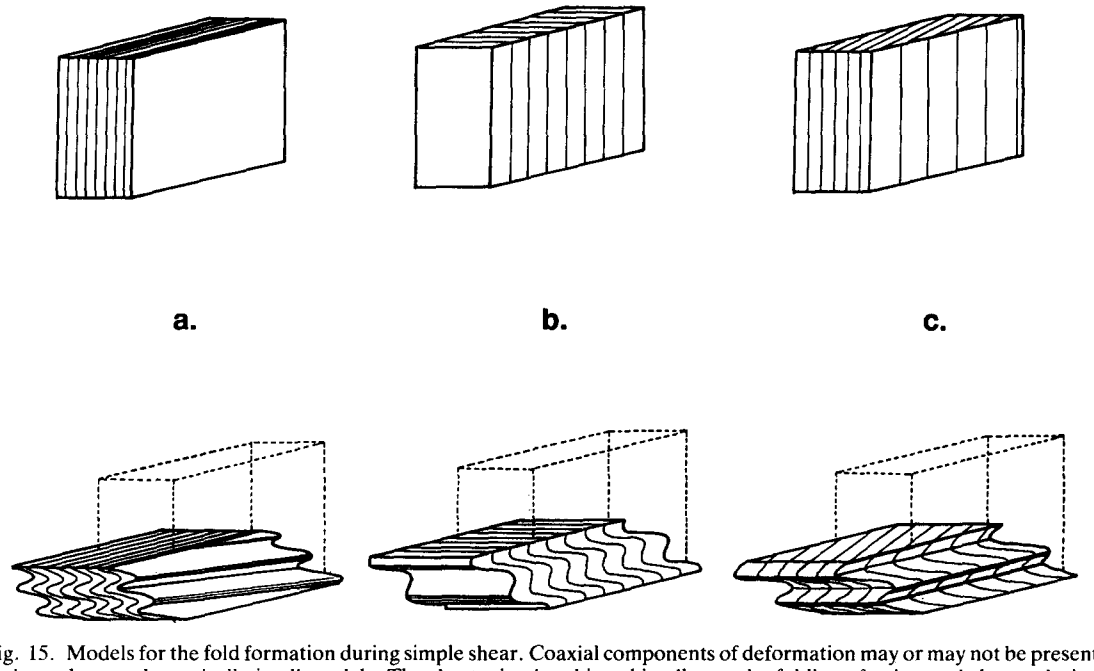


Fig. 15. Models for the fold formation during simple shear. Coaxial components of deformation may or may not be present and are shown schematically in all models. The shortening is achieved in all cases by folding of anisotropic layers during concomitant simple shear deformation. (a) Anisotropy perpendicular to the shear plane and parallel to the shear direction. (b) Anisotropy at a high angle to the shear direction and to the shear plane. (c) Anisotropy inclined to the shear direction and perpendicular to the shear plane.

of the finite strain ellipsoid (Escher & Watterson 1974). Such a situation is suggested for fold sample 3 and is similar to a fold model proposed by Nicolas & Boudier (1975). However, it differs from their model in that it does not involve constrictional deformation.

In fold sample 1 the fold axis is approximately perpendicular to the shear direction. The fold probably represents a case, like the second model (Fig. 15b), which is again drawn as a combination of simple shear and coaxial deformation. The coaxial components may or may not be present. The orientation of the axial plane depends on the orientation of the shortening direction with respect to the shear direction. However, the orientation of the axial plane of folds generated in model experiments in a simple shear environment (without coaxial shortening) does not always appear to be fixed with respect to the shear plane or the finite strain $XY$ plane (Manz & Wickham 1978). The axial plane is shown schematically parallel to the shear plane in Fig. 15(b). In such a model, it is not easily explained why the fold axis should not be rotated towards the shear direction. One explanation could be that the finite simple shear strain is not high enough to cause an extensive rotation of the fold axis, because large shear strains are required for that (Skjernaa 1980).

If the anisotropy plane is orientated at an angle to the shear direction, and at a high angle to the shear plane, the geometric configuration may be expected to be a combination of the ones described above. The buckling of the layers is expected to occur in such a way that the fold axes are oblique to the shear direction (Fig. 15c). The orientation of the axial plane is difficult to assess in such a case. The angle of the fold axes with respect to the shear direction may cause an inclination of the axial plane with respect to the $XY$ plane of the finite strain ellipsoid. Such an inclined fold axis situation probably can explain the folds of sample 2, because the inclination of the fold axis in sample 2 does not appear to be the result of an extensive rotation of the fold axis towards the shear direction. The flexural-slip component in these layers during the folding lies in the $XZ$ plane of the finite strain ellipsoid. In this geometrical configuration of folding and shear deformation (Fig. 15c), a stretching lineation, which is then folded by flexuring of the limbs, can form and remain in the $XZ$ plane of the finite strain ellipsoid.

Generally, all three models take into account the fact that the fold geometry and fold orientation may largely be a result of the original orientation of the anisotropy with respect to the shortening or shear direction (Talbot 1970, Escher & Watterson 1974, Skjernaa 1980). A variable original orientation of the anisotropy probably causes the variable fold axis orientation with respect to the shear directions in these folds. Larger scale examples of folds initially oblique to the shear direction have been described by Malavieille (1987). A major problem, namely why the fold axes do not rotate substantially towards the extension direction, remains difficult to explain. However, as pointed out above, the treatment of fold axes as mechanically passive lines during rotation (Sanderson 1973, Escher & Watterson 1974, Cobbold & Quinquis 1980, Skjernaa 1980) may not apply to the case described here.

*Acknowledgements*—This work has benefited greatly from many discussions with Martin Casey, Stefan Schmid and Renee (Panozzo) Heilbronner. Guido Schreurs carried out the X-ray texture goniometry. Stefan Schmid and John Ramsay substantially improved earlier versions of the manuscript by their critical reviews and good suggestions. Renee (Panozzo) Heilbronner, Stefan Schmid and Simon Hanmer critically reviewed the final version. Alex McLaren improved the English. Paul Brugman did some of the drafting. I would like to thank them all very much for their help. This work was supported by ETH Credit No. 0.330.084.46/8 and National Fonds Project No. 5.521.330.739/8.

## REFERENCES

Bak, J., Korstgård, J. & Sørenson, K. 1975. A major shear zone within the Nagssugtoqidian of West Greenland. *Tectonophysics* **27**, 191–209.

Ball, T. K. 1960. A petrofabric analysis of a fold. *Am. J. Sci.* **258**, 274–281.

Berthé, D. & Brun, J.-P. 1980. Evolution of folds during progressive shear in the South Armorican Shear Zone, France. *J. Struct. Geol.* **2**, 127–133.

Bouchez, J. C. & Pêcher, A. 1981. The Himalayan Central Thrust pile and its quartz-rich tectonites in Central Nepal. *Tectonophysics* **78**, 23–50.

Brunel, M. 1980. Quartz fabrics in shear zone mylonites: evidence for a major imprint due to late strain increment. *Tectonophysics* **64**, T33—T34.

Burg, J.-P. 1986. Quartz shape fabric variation and *c*-axis fabrics in a ribbon-mylonite: arguments for an oscillatory foliation. *J. Struct. Geol.* **8**, 123–131.

Carreras, J., Estrada, A. & White, S. 1977. The effects of folding on the *c*-axis of a quartz mylonite. *Tectonophysics* **39**, 3–24.

Casey, M. & Huggenberger, P. 1985. Numerical modeling of finite-amplitude similar folds developing under general deformation histories. *J. Struct. Geol.* **7**, 103–114.

Cobbold, P. R. & Quinquis, 1980. Development of sheath folds in shear regimes. *J. Struct. Geol.* **2**, 119–126.

Cobbold, P. R. & Watkinson, A. J. 1981. Bending anisotropy: a mechanical constraint on the orientation of fold axes in an anisotropic medium. *Tectonophysics* **72**, T1–T10.

Dell'Angelo, L. N. & Tullis, J. 1986. A comparison of *c*-axis preferred orientations in experimentally deformed aplites and quartzites. *J. Struct. Geol.* **8**, 683–692.

Dell'Angelo, L. N. & Tullis, J. 1989. Fabric development in experimentally sheared quartzites. *Tectonophysics* **169**, 1–21.

Dhonau, T. J. 1961. The relation between the quartz fabric and fold movements in a folded calc-silicate rock from Moines of Scotland. *Geol. Mag.* **98**, 313–316.

Escher, A. & Watterson, J. 1974. Stretching fabrics, folds and crustal shortening. *Tectonophysics* **22**, 223–231.

Gangopadhyay. P. K. & Johnson, M. R. W. 1962. A study of quartz orientation and its relation to movements in shear folds. *Geol. Mag.* **99**, 69–84.

Garcia Celma, A. 1982. Domainal and fabric heterogeneities in the Cap de Creus quartz mylonites. *J. Struct. Geol.* **4**, 443–455.

Garcia Celma, A. 1983. *C*-axis and shape fabrics in quartz in mylonites of Cap de Creus Spain: their properties and development. Unpublished Ph.D. thesis, University of Utrecht.

Ghosh, S. K. & Ramberg, H. 1968. Buckling experiments on intersecting fold patterns. *Tectonophysics* **5**, 89–105.

Hanmer, S. K. 1984. Strain-insensitive foliations in polymineralic rocks. *Can. J. Earth Sci.* 21, 1410–1414.

Hara, J. 1971. An ultimate steady state pattern of *c*-axis fabric of quartz in metamorphic tectonites. *Geol. Rdsch.* **60**, 1142–1173.

Jessel, M. W. 1986. Grain boundary migration and fabric development in experimentally deformed octachloropropane. *J. Struct. Geol.* **8**, 527–542.

Jones, K. A. 1959. A petrofabric method of fold analysis. *Am. J. Sci.* **257**, 138–143.

Knipe, R. J. & Law, R. J. 1987. The influence of crystallographic orientation and grain boundary migration on microstructural and textural evolution in an *S–C* mylonite. *Tectonophysics* **135**, 155–169.

Ladurner, J. 1951. Beiträge zur Typisierung von Quarzfalten. *Tscherm. Min. Pet. Mitt.* 3. *Folge* **2**, 47–66.

Law, R. J., Casey, M. & Knipe, R. J. 1986. Kinematic and tectonic significance of microstructure and crystallographic fabrics within quartz mylonites from the Assynt and Eriboll regions of the Moine thrust zone, NW Scotland. *Trans. R. Soc. Edin., Earth Sci.* **77**, 99–125.

Lister, G. S. & Dornsiepen, U. F. 1980. Fabric transitions in the Saxony Granulite Terrain. *J. Struct. Geol.* **4**, 81–92.

Lister, G. S. & Snoke, A. W. 1984. *S–C* mylonites. *J. Struct. Geol.* **6**, 617–638.

Malavieille, J. 1987. Extensional shearing deformation and km-scale "a"-type folds in a Cordilleran metamorphic core complex (Raft River Mountains, NW-Utah). *Tectonics* **6**, 423–448.

Manz, R. & Wickham, J. 1978. Experimental analysis of folding in simple shear. *Tectonophysics* **44**, 79–90.

Means, W. D. 1981. The concept of steady state foliation. *Tectonophysics* **78**, 179–199.

Means, W. D. 1983. Microstructure and micromotion in recrystallization flow of octochloropropane: a first look. *Geol. Rdsch.* **72**, 511–528.

Nicolas, A. & Boudier, F. 1975. Kinematic interpretation of folds in alpine-type peridotites. *Tectonophysics* **25**, 233–260.

Panozzo, R. 1983. Two dimensional analysis of shape fabric using projections of lines in a plane. *Tectonophysics* **95**, 279–294.

Panozzo, R. 1984. Two dimensional strain from the orientation of lines in a plane. *J. Struct. Geol.* **6**, 215–221.

Passchier, C. W., Urai, J. L., van Loon, J. & Williams, P. F. 1981. Structural geology of the Central Sesia Lanzo Zone. *Geologie Mijnb.* **60**, 497–507.

Price, G. P. 1981. Application of the photometric method to fabric mapping around folds. *Tectonophysics* **78**, 85–100.

Ralser, S. 1987. Experimental deformation of a quartz mylonite. Unpublished Ph.D. thesis, Monash University.

Ramsay, J. G. 1960. The deformation of early linear structures in areas of repeated folding. *J. Geol.* **68**, 75–93.

Ramsay, J. G. 1962. The geometry and mechanics of formation of "similar" type folds. *J. Geol.* **70**, 309–327.

Ramsay, J. G. 1967. *Folding and Fracturing of Rocks*. McGraw-Hill, New York.

Ramsay, J. G. & Huber, M. I. 1987. *The Techniques of Modern Structural Geology, Volume* 2: *Folds and Fractures*. Academic Press, London.

Rhodes, S. & Gayer, R. A. 1977. Non-cylindrical folds, linear structures in the *X*-direction and mylonite development during translation of the Caledonian Kalak Nappe Complex of Finnmark. *Geol. Mag.* **114**, 329–408.

Sander, B. 1931. *Gefügekunde der Gesteine*. Springer, Wien.

Sanderson, D. J. 1973. The development of fold axes oblique to the regional trend. *Tectonophysics* **16**, 55–70.

Schmid, S. M. & Casey, M. 1986. Complete fabric analysis of some commonly observed quartz *c*-axis patterns. *Am. Geophys. Un. Geophys. Monogr.* **36**, 263–286.

Schmid, S. M., Panozzo, R. & Bauer, S. 1987. Simple shear experiments on calcite rocks: rheology and microfabric. *J. Struct. Geol.* **9**, 747–778.

Simpson, C. & Schmid, S. M. 1983. An evaluation of criteria to deduce the sense of movement in sheared rocks. *Bull. geol. Soc. Am.* **94**, 1281–1288.

Skjernaa, L. 1975. Experiments on superimposed buckle folding. *Tectonophysics* **27**, 255–270.

Skjernaa, L. 1980. Rotation and deformation of randomly oriented planar and linear structures in progressive simple shear. *J. Struct. Geol.* **2**, 101–109.

Stünitz, H. 1989. Partitioning of metamorphism and deformation in the boundary region of the "Seconda Zona Diorito-Kinzigitica", Sesia Zone, Western Alps. Unpublished Ph.D. thesis, ETH, Zurich.

Talbot, C. J. 1970. The minimum strain ellipsoid using deformed quartz veins. *Tectonophysics* **9**, 47–76.

Urai, J. L. 1983. Deformation of wet salt rocks. Unpublished Ph.D. thesis, University of Utrecht.

Urai, J. L., Means, W. D. & Lister, G. S. 1986. Dynamic recrystallization of minerals. *Am. Geophys. Un. Geophys. Monogr.* **36**, 161–199.

Watkinson, A. J. 1981. Patterns of fold interference: influence of early fold shapes. *J. Struct. Geol.* **3**, 19–23.

Watkinson, A. J. & Cobbold, P. R. 1981. Axial directions of folds in rocks with linear/planar fabrics. *J. Struct. Geol.* **3**, 211–217.

Wilson, C. J. L. 1986. Deformation induced recrystallization of ice: The application of in-situ experiments. *Am. Geophys. Un. Geophys. Monogr.* **36**, 213–232.